Soliton Order Preservation for Self-frequency Shift with High Efficiency and Broad Tunability

Md Hosne Mobarok Shamim, Imtiaz Alamgir, and Martin Rochette, *Senior Member, IEEE*

***Abstract*— We present a soliton order preservation mechanism leading to broad tunability with high energy conversion efficiency (ECE) from a fiber-based soliton self-frequency shift (SSFS) system. Here, a pulse compressing fiber, placed before the Raman shifting nonlinear fiber (NLF), acts as a soliton order preserver. Thanks to this passive mechanism, the soliton order at the input of the NLF is preserved within 2.0<*N*<2.3 despite a ~6.7-fold energy increase. The resulting pulse leads to an SSFS that is spectrally tunable over 1.96-2.14 µm while keeping an ECE of 80-85%. It is the first time that an ECE>80% is maintained over a tunable range as large as 180 nm in a passive fiber-based SSFS system. Solitons are also tunable up to 320 nm in the wavelength range of 1.96-2.28 µm with ECE>50%. Such a soliton order preservation mechanism that enables a high ECE while maintaining a broad soliton tunability is of utmost practical interest for wavelength conversion systems.**

***Index Terms*— Optical solitons, fiber nonlinear optics, thulium doped fiber amplifier, soliton self-frequency shift**

I. Introduction

Soliton self-frequency shift (SSFS) is a well-known wavelength conversion process that generates femtosecond pulses with broad spectral tunability [1]–[4]. In the 2 µm wavelength band, SSFS has been demonstrated on one hand from passive fibers, and on the other hand from active fibers. In passive systems, an optical pump pulse is injected at the input of a nonlinear fiber (NLF) to become a high-order soliton (or mother soliton) that fissions into several fundamental solitons, and each of them experiences variable amounts of SSFS. The soliton that spectrally shifts the most is the one used for wavelength conversion. This SSFS process is tuned by adjustment of the pump power [5]. As power is increased, the mother soliton of increasing order N transfers energy to an increasing number N of fundamental solitons, reducing the fraction of energy provided to the soliton that spectrally shifts the most. Hence, as the pump power increases, SSFS increases but energy conversion efficiency (ECE), defined as the ratio of the energy of the red shifted soliton to the total output energy, decreases. It results a trade-off in between SSFS tunability and ECE [6]–[10].

Passive fibers lead to simple SSFS systems, but it is a challenge to reach broad SSFS tunability while preserving a high ECE. For instance, Fang *et al.* have demonstrated SSFS with a tunability of 40 nm in the wavelength range of 1.70-1.74 µm, resulting in an ECE of 76%-80% [11]. Morin *et al.* reported a comparatively larger tunability of 350 nm in the wavelength range of 1.70-2.05 µm, resulting in an ECE of 50%-75% [12]. It is evident from these results that increased SSFS tunability is available at the cost of decreasing ECE.

In contrast to passive fibers, active fibers such as thulium-doped fiber amplifiers (TDFA), also acting as NLF, have led to SSFS tunability as large as 300 nm while maintaining an ECE as high as 90% [13]–[16]. To enable this, the pump pulse is pre-chirped prior to SSFS in the TDFA, implemented from an optimized length of dispersion compensating fiber (DCF) [15], [16]. It however remains unclear how pre-chirping acts to enable a broad SSFS tunability while maintaining a high ECE. A better understanding of the link between pre-chirp and high ECE would serve to optimize SSFS systems, whether the systems are based on active fibers or passive fibers.

In this work, we introduce soliton order preservation, a mechanism enabled by high-order soliton compression effect in a pulse compressing fiber (CF) which allows the soliton order at the input of the NLF to be preserved within a certain range while the energy of the mother soliton increases. We analyze how a pre-chirped pulse affects this mechanism and use this knowledge to design an SSFS system that enables broad tunability while maintaining a high ECE. We experimentally show that the energy of a mother soliton can be increased ~6.7-fold while remaining within a narrow order range of 2.0<N<2.3 by an interplay of pump chirp, duration, and peak power. This mother soliton is used to demonstrate an SSFS with a tunability of 180 nm in the wavelength range of 1.96-2.14 µm while maintaining an ECE>80%. The tunability of the system is extended to 320 nm in the wavelength range of 1.96-2.28 µm while maintaining ECE>50%. Such a soliton order preservation mechanism that enables a high ECE while maintaining a broad soliton tunability is of utmost practical interest for wavelength conversion systems.

II. Experimental Setup

Fig. 1(a) is a schematic of the proposed SSFS system. A thulium-doped fiber laser (TDFL, AdValue Photonics AP-ML) is used as the seed source. It generates pulses with a duration of

Manuscript received ** 2022; revised July **, 2022; accepted July **, 2022. Date of publication January **, ****; date of current version July **, ****. Authors acknowledge the support from the Natural Sciences and Engineering Research Council of Canada.

M. H. M. Shamim, I. Alamgir and M. Rochette are with the Department of Electrical and Computer Engineering, McGill University, 3480 University Street, Montréal, H3A 0E9, QC, Canada. (Corresponding author: e-mail: hosne.shamim@mail.mcgill.ca).

Color versions of one or more of the figures in this letter are available online at http://ieeexplore.ieee.org.

Digital Object Identifier 10.1109/JLT.****.*******

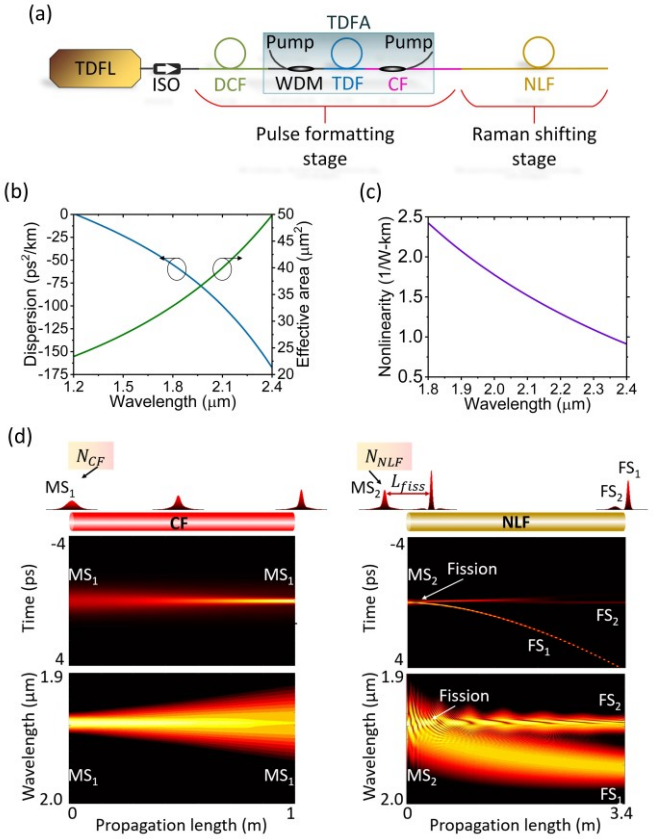

Fig. 1. (a) Experimental setup for wavelength conversion. TDFL: thulium-doped fiber laser; ISO: isolator; DCF: dispersion compensating fiber; WDM: wavelength division multiplexer; TDF: thulium doped fiber; CF: compressing fiber; TDFA: thulium-doped fiber amplifier; NLF: nonlinear fiber. (b) Group velocity dispersion and effective area and (c) nonlinearity of the NLF. (d) Temporal and spectral evolution of the soliton in the CF and the NLF.

900 fs, a repetition rate of 30 MHz, and an average power of 6.5 mW corresponding to a pulse energy of 217 pJ, at a wavelength of 1.94 μm. An isolator (ISO) after the TDFL ensures the unidirectional propagation of light in the system. Pulses from the seed laser are then propagated through a pulse formatting stage and a Raman shifting stage. The pulse formatting stage consists of a DCF and a homemade TDFA. The TDFA boosts the pulses in a 32 cm long thulium doped fiber (TDF, Coractive DCF-TM-6/125) which is pumped by up to 2.7 W of C-band light from two erbium-doped fiber amplifiers (EDFAs) in the co-propagating and counter propagating directions via two wavelength division multiplexers (WDMs). Before amplification in the TDFA, the chirp of pulses is adjusted by varying the length of a DCF (Nufern UHNA7) from 7.5 m to 8.5 m, which exhibits a normal group velocity dispersion (GVD) $\beta_{2,DCF}$=43 ps^2/km at the pump wavelength [17]. After amplification, a second WDM works as a CF with a length of 1 m, $\beta_{2,CF}$=- 76 ps^2/km, and nonlinearity γ_{CF}=0.8 W^{-1} km^{-1} at the pump wavelength. The isolator and WDMs have insertion losses of 1.2 dB and 1.0 dB, respectively. The isolator has 1.5 m long pigtails of standard single-mode fibers (SSMF) on each side. The fiber to fiber coupling of DCF with SSMF, and TDF with SSMF is not optimized for low loss and leads to a loss of 3 dB/connection. In the Raman shifting stage, a silica based nonlinear fiber (NLF, Coractive SCF-UN) is used with core/cladding diameters of 6/125 μm and a numerical aperture of 0.23. It is fusion spliced with the CF with an insertion loss of 1.4 dB, i.e. with a transmittance Γ=72%. The length of NLF is first estimated from the modified Gordon's formula [1] and then experimentally optimized to 3.4 m to maximize SSFS. Fig. 1(b) shows the wavelength dependent GVD and effective mode area of the NLF, calculated from solving the characteristic equation of the fundamental mode in an optical fiber [18]. Fig. 1(c) shows the calculated nonlinearity of the NLF. The nonlinear refractive index at the pump wavelength of 1.94 μm is ~2.5×10^{-20} m^2/W, extracted from an interpolation of experimental results from [19] and [20]. At the pump wavelength, the NLF has a GVD $\beta_{2,NLF}$=- 74 ps^2/km, an effective mode area of 36 μm^2 and nonlinearity γ_{NLF}=2.2 W^{-1} km^{-1}. The output of the NLF is probed with a power meter (Newport 843-R), an intensity autocorrelator (Femtochrome research FR-103XL), and an optical spectrum analyzer (OSA, Yokogawa AQ6375B).

Fig. 1(d) illustrates the temporal and spectral evolution of the soliton in the CF and NLF. The amplified pulse coming from the TDF forms a mother soliton (MS$_1$) of order N_{CF} at the CF input. MS$_1$ undergoes a power and chirp dependent nonlinear compression in the CF. Passing from CF to NLF, MS$_1$ is converted into MS$_2$ because of the unequal fiber parameters. In the NLF, MS$_2$ experiences fission due to high-order Raman and GVD effects, leading to two stable fundamental solitons, FS$_1$ and FS$_2$, when the order of MS$_2$ is 1.5<N_{NLF}<2.5. FS$_1$ being the most powerful soliton and having the shortest duration experiences the most SSFS, precisely determined by its peak power, duration, chirp, and fiber properties [1], while FS$_2$ mostly remains at the pump wavelength.

III. Relation between Energy Conversion Efficiency and Soliton Order

The soliton order is defined

$$N = \sqrt{\gamma \tau^2 P_0 / |\beta_2|} \quad (1)$$

where τ is the pulse duration and P_0 is the peak pulse power. Numerical simulations are performed by solving the generalized nonlinear Schrodinger equation, to highlight the relation between the order of MS$_2$ and the ECE of FS$_1$ [2]. GVD up to 7th order of Taylor's series, Raman time response, and self-steepening are considered. Pulses having a full width at half maximum (FWHM) duration from 50 fs to 550 fs with 50 fs interval are considered for the simulation. The peak powers are adjusted so that N of the MS$_2$ varies from 1 to 5. In the NLF, MS$_2$ undergoes spectral broadening and temporal compression when N_{NLF}≥1.5 before it fissions after travelling a distance, $L_{fiss} \sim L_D / N_{NLF}$, where $L_D = \tau^2 / |\beta_{2,NLF}|$ is the dispersion length [21]. For all combinations of duration and order of MS$_2$, L_{fiss} varies in between 7 mm when N_{NLF}=5 and τ=50 fs, to 2.2 m when N_{NLF}=1.5 and τ=500 fs.

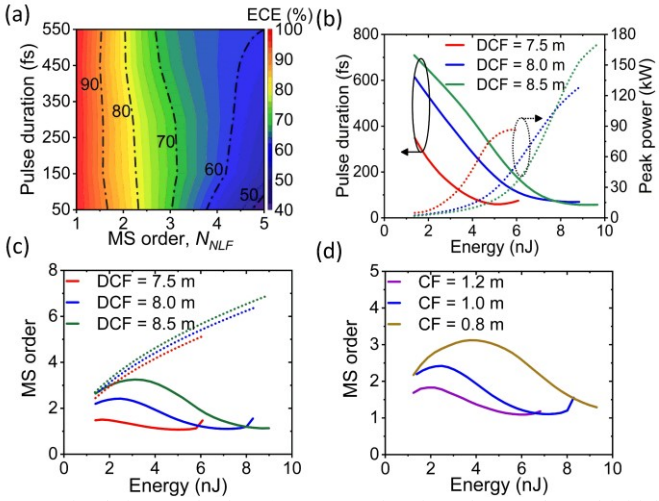

Fig. 2. Simulation results for (a) ECE as a function of MS order and initial pulse duration. (b) Duration and peak power of MS_1 at the CF output as a function of energy. (c) N_{CF} (dotted lines) and N_{NLF} (solid lines) as a function of energy. (d) N_{NLF} as a function of energy and CF length when DCF length is 8.0 m.

Fig. 2(a) shows the ECE as a function of N_{NLF} and duration of MS_2. It is observed that the order of MS_2 should maintain N_{NLF} <2.4, almost independently of its duration, to ensure an ECE>80%. In contrast, the ECE would be increased to 90-100% at the expense of a reduced SSFS for N_{NLF}<1.5.

IV. Soliton Order Preservation

The SSFS process is tuned by varying the energy of the pump pulse. In conventional SSFS systems with passive fibers, this is performed by varying the peak power of a pulse prior to entering the NLF using an attenuator. Here, it is instead the energy of the pump pulse that is varied while ensuring that MS_2 preserves N_{NLF}<2.4 from a combination of peak power, pulse duration, and chirp of MS_1. The DCF pre-chirps the pulse before amplification and determines the pulse compression in the CF. Numerical simulations are performed to observe how the pulse compression is affected as the lengths of DCF and CF are varied, and their impact on N_{NLF}.

A temporal soliton in the form of $A(z,t) = \sqrt{P_0}\,\mathrm{sech}(t/\tau)\exp(-iCt^2/2\tau^2)$, where C is the chirp parameter, is numerically propagated through a 3 m length of SSMF (ISO) followed by three variable DCF lengths of 7.5 m, 8.0 m, and 8.5 m, and a 1 m long SSMF (WDM) [2]. The pulse is initially chirp-free (C =0) but accumulates chirp with propagation up to reaching the TDF. The values of C =2.69, 2.89, and 3.02 for the three DCF lengths, respectively, are extracted from the pulse using

$$C = -\tau\left(\frac{d^2\phi}{dt^2}\right) \tag{2}$$

Here, τ is the pulse duration and ϕ is the phase of the pulse after propagation. After the TDF, the amplified pulse is sent to the CF at varying peak powers to emulate the effect of the energy dependent pulse compression process. Fig. 2(b) show the FWHM duration and the corresponding peak power of the compressed MS_1 with varying energy. The soliton is compressed 5.9-fold from 348 fs to 59 fs, 8.9-fold from 612 fs to 69 fs, and 12.4-fold from 709 fs to 57 fs for DCF lengths of 7.5 m, 8.0 m, and 8.5 m, respectively. The compression factor depends on the value of N_{CF} [22].

Fig. 2(c) shows the order of MS_1 at the CF entrance (N_{CF}) as a function of TDFA energy, for the three DCF lengths. The increase of N_{CF} is proportional to the square root of the energy, as expected from Eq. (1). Fig. 2(c) also shows the order of MS_2 at the NLF input N_{NLF} as a function of DCF length. The N_{NLF} can be written as,

$$N_{NLF} = \sqrt{\Gamma P_0 \tau^2 \gamma_{NLF}/|\beta_{2,NLF}|} \tag{3}$$

The duration and peak power are taken from the output of the CF as shown in Fig. 2(b) and serve as an estimate for N_{NLF} of the mother soliton that results after shedding of dispersive waves. This estimate provides an accurate number of fundamental solitons that may appear after the fission in the NLF. As the energy increases, N_{NLF} increases until it reaches a plateau from which it then starts to decrease, thus preserving the soliton order under a maximum limit. The preservation of the soliton order originates from the interplay of pulse duration and peak power of the compressed MS_1 [23]. The minimum of N_{NLF} corresponds to a point of maximum pulse compression from the CF. Increasing the energy even more would lead to the fission of MS_1 in the CF, thus resulting into an end to the preservation in the NLF. The soliton order in the NLF is preserved within $1.0<N_{NLF}<1.5$, $1.1<N_{NLF}<2.4$, and $1.2<N_{NLF}<3.2$ for DCF lengths of 7.5 m, 8.0 m, and 8.5 m, respectively. The range of values taken by N_{NLF} as a function of power is dictated by the initial duration and chirp of the MS_1 as well as the length of the CF. Fig. 2(d) shows the impact of CF length on soliton order preservation. For this, the DCF length is fixed at 8.0 m and the CF length is varied from 0.8 m to 1.2 m with 0.2 m interval. Minimum order of MS_1 occurs for relatively smaller amount of average power when CF length is 1.2 m compared to 0.8 m. Since longer propagation length in CF allows more compression for a given amount of energy, N_{NLF} generally decreases with increased CF lengths [22]. From this result, the length of the CF is another way to ensure that N_{NLF} remains bounded as a function of energy.

V. Experimental Results and Discussion

The soliton order preservation is verified next from the experimental setup. For this purpose, the energy of the seed pulse is increased by up to 6.7 times in the TDFA from 1.3 nJ

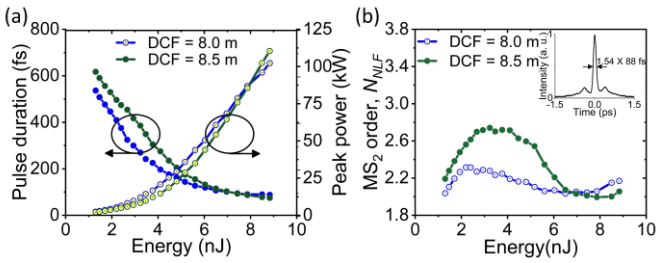

Fig. 3. (a) Measured pulse duration and peak power of MS_1 and (d) measured N_{NLF} when the DCF length is 8.0 m and 8.5 m.

This article has been accepted for publication in IEEE/OSA Journal of Lightwave Technology. This is the author's version which has not been fully edited and content may change prior to final publication. Citation information: DOI 10.1109/JLT.2022.3223802

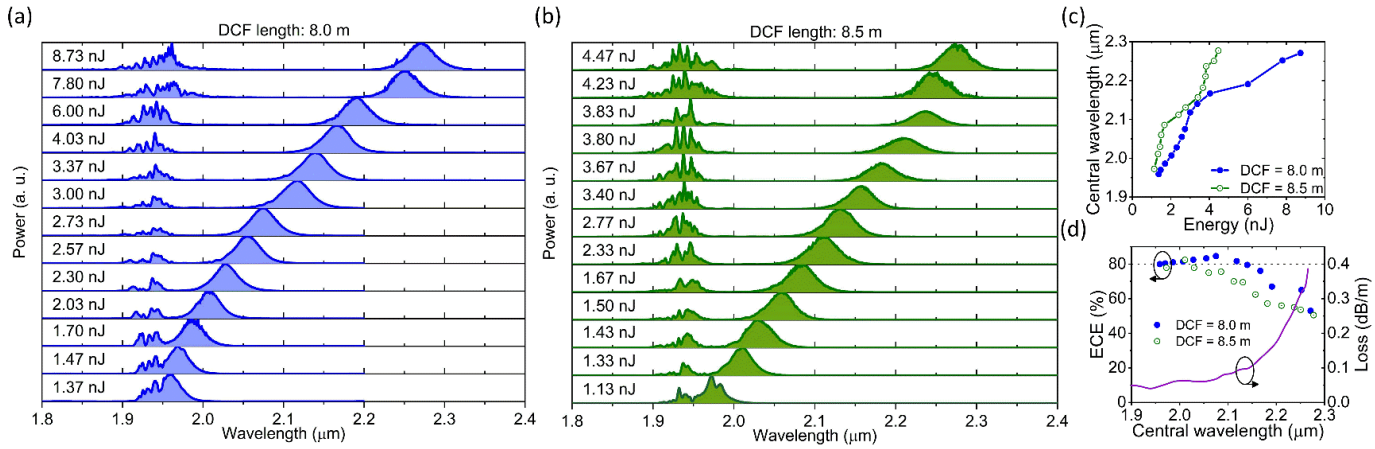

Fig. 4 Experimental spectrum evolution at the output of the NLF as a function of average pump power to the NLF for a DCF length of (a) 8.0 m and (b) 8.5 m. (c) central wavelength of the soliton as a function of the energy and (d) measured ECE and transmission loss of the NLF as a function of the soliton central wavelength.

to 8.7 nJ and propagated in the CF. The duration and peak power of the compressed pulse is measured at the CF output. For this experiment, a CF length of 1.0 m and DCF lengths of 8.0 m and 8.5 m are considered. Fig. 3(a) shows the FWHM duration and peak power of MS_1. For a DCF length of 8.0 m, MS_1 is temporally compressed from 536 fs to 88 fs with peak power increasing from 2.4 kW to 102 kW. For DCF length of 8.5 m, MS_1 is compressed from 622 fs to 81 fs and the peak power increases from 2.1 kW to 110 kW. The duration and peak power of the compressed MS_1 closely matches the simulation results as shown in Fig. 2(b). The inset of Fig. 3(b) shows the autocorrelation trace of the pulse at its maximum compression level for DCF length of 8.0 m. In the trace, the appearance of a pedestal is a well-known characteristic of solitonic pulse compression systems [23]. Fig. 3(b) shows the measured value of N_{NLF} as a function of the MS_1 energy. The soliton order is preserved within $2.0< N_{NLF} <2.3$ and $2.0< N_{NLF} <2.7$ for the DCF lengths of 8.0 m and 8.5 m, respectively, despite ~6.7 folds increase of the energy. The measured values are in good agreement with the simulated values shown in Fig. 2(c). A minor difference between them may be explained from the simulation that neglects nonlinear effects in the TDF.

Fig. 4(a) and (b) present output spectra from the NLF as a function of average pump power for a DCF length of 8.0 m and 8.5 m, respectively. The spectra show a self-shifting fundamental soliton and its residual power at the pump wavelength. The pump residue in the first case is relatively smaller than the second case confirming that in the former, the N_{NLF} is preserved at a lower value, as expected from Fig. 3(b). Fig. 4(c) compares the central wavelength of the tunable solitons as a function of the average pump power for these two cases. With a DCF length of 8.0 m, the soliton is tunable in the wavelength range of 1.96-2.27 μm from an average pump power variation from 1.37 nJ to 8.73 nJ. With a DCF length of 8.5 m, the soliton is tunable over almost the same spectral range (1.97-2.28 μm), but using a pump power variation from 1.13 nJ to 4.46 nJ. With respect to the pump power, the rate of SSFS of the later is higher than the former. It can be explained from the distribution of energy after the fission process. High order MS fissions into FSs with shorter pulses leading to a larger frequency shift [1]. Since for the second case, the value of N_{NLF} is higher as a function of pump power, it is expected that the rate of SSFS will be higher as well. Fig. 4(d) compares the ECE as a function of soliton central wavelength. ECE is calculated using the spectral integral method[13], [15], [24], [25]. For DCF length of 8.0 m, the ECE remains >80% over a tuning range of 1.96-2.14 μm (180 nm), and it varies in the range of ECE=85-53% over the overall tuning range of 1.96-2.27 μm. For DCF length of 8.5 m, ECE >70% over a tuning range of 1.97-2.13 μm (160 nm), and it varies in the range of ECE=82-51% over the available tuning range of 1.97-2.28 μm. Compared to the DCF length of 8.5 m, 8.0 m yields enhanced ECE for similar frequency shift at relatively high power. In both cases, the ECE is preserved with increasing pump power. This agrees with the findings of Fig. 2(c). An ECE>80% for a tuning window as broad as 180 nm (12.9 THz) has never been reported in passive fibers, irrespective of the wavelength of operation. Additionally, to the best of our knowledge, the maximum ECE=85% obtained in this experiment is the highest reported value from a passive fiber based SSFS system. The high-ECE over a broad spectral range of tunability obtained in this experiment is attributed to the soliton order that is limited to N_{NLF}<2.4, thanks to the energy-dependent soliton compression in the CF. In both cases, further frequency shift and the reduction of ECE beyond 2.15 μm are attributed to silica losses in the NLF (see fig. 4(d)). DCF length of 8.0 m is advantageous over 8.5 m for high ECE wavelength conversion and a better precision on wavelength tuning since it is spread over a larger power variation. However, the DCF length of 8.5 m is interesting for low power consumption. Since the objective of this study is to obtain high ECE with broad tunability, only the DCF length of 8.0 m is considered for further characterization of the system. SSFS to wavelengths in excess of 2.39 μm is also achieved (not shown) by increasing the pump energy, but this leads to the generation of more than two solitons and sudden reduction in ECE.

Numerical simulations were performed to reproduce the experimental data. The wavelength dependent propagation loss of the NLF (Fig. 4(d)) is considered in the simulations. The peak powers and durations of the MS_2 are derived from Fig. 3(a). The chirp parameter of MS_2 at the NLF input is

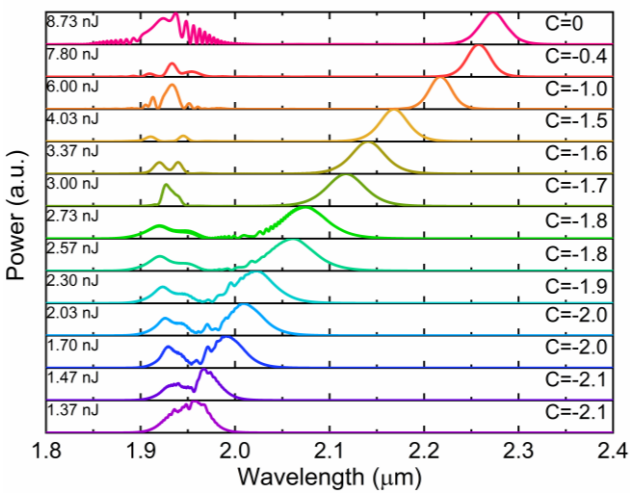

Fig. 5 Numerical spectrum evolution at the output of the NLF as a function of energy to the NLF. The chirp parameter (C) indicates initial chirp of the MS_2 chosen from numerical simulation for the best fit with the experimental results.

evaluated at every power levels for the best fit with experimental results. In the experiment, the chirp of MS_2 originates from an interplay of dispersion and nonlinear effects of MS_1 in the CF [22]. At maximum compression, chirp due to dispersion and nonlinear effects cancel each other and becomes zero. Since in this case the DCF is optimized for maximum compression at ~8.73 nJ, solitons experience a chirp when the pump power is lower than the optimal value [22]. Fig. 5 depicts the simulated evolution of solitons. At an energy of 1.37 nJ, a soliton emerges and experiences SSFS after having shed dispersive waves. As the energy is increased, the soliton undergoes an increased amount of SSFS caused by an increased peak power and reduced pulse duration. At an energy of 8.73 nJ, the soliton reaches a wavelength of 2.27 μm. A good fit is achieved between the simulated and experimental soliton spectra of Fig. 4(a), when the initial chirp parameter of MS_2 is varied from -2.1 to 0 as the energy increases from 1.37 nJ to 8.73 nJ.

Fig. 6 shows the optical spectrum (Fig. 6a) and autocorrelation trace (Fig. 6b) of the filtered soliton along with a $sech^2$ profile fitting centered at a wavelength of 2.14 μm. The FWHM spectral width and the duration of the soliton is 39.8 nm and 134 fs, respectively, resulting in a time-bandwidth product (TBP) of 0.35, indicating almost a chirp-free ideal soliton. The measurement of the soliton duration is limited up to 2.2 μm because of the low sensitivity of the autocorrelator beyond this wavelength. All the soliton up to this wavelength has a

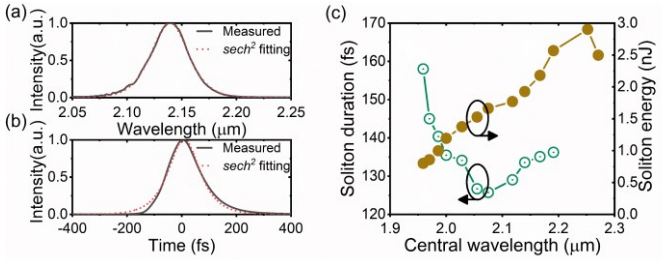

Fig. 6. Measured (a) spectrum and (b) autocorrelation trace of the wavelength converted soliton superimposed with the $sech^2$ profile. Measured (c) soliton duration and (d) soliton energy as a function of central wavelength.

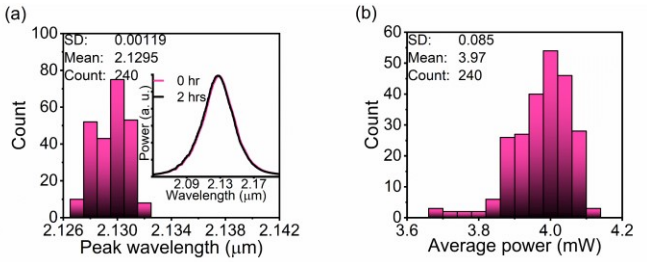

Fig. 7. Statistical distribution of (a) peak wavelength and (b) average power of the soliton at a wavelength of 2.13 μm over a duration spread of 2 hours. SD: standard deviation; Count: number of data sample.

TBP<0.39.

Fig. 6(c) shows the measured duration and energy of the wavelength converted soliton as a function of wavelength. The soliton duration and energy vary from 126 fs to 158 fs and 0.8 nJ to 2.9 nJ, respectively. The minimum soliton duration and maximum energy occur at a wavelength of 2.12 μm and 2.25 μm, respectively. The soliton energy remains above 1 nJ in the wavelength range of 1.99-2.27 μm, which is a relatively large energy for solitons emerging from small core silica NLF. Increasing energy of the soliton is associated with the required increasing pump for SSFS to reach longer wavelengths. The sudden decrease of soliton energy at the wavelength of 2.27 μm is attributed to the increasing transmission loss of the NLF.

Finally, the soliton at a (mid-range) SSFS wavelength of 2.13 μm is observed for two hours to assess the stability of the system. For this purpose, the SSFS spectrum is recorded with the OSA with a periodic interval of 30 seconds, from which the central wavelength and average power of the soliton are extracted. Figs. 7(a) and (b) show the statistical analysis of the 240 recorded samples. The inset of Fig. 7(a) shows that the soliton spectrum recorded at the beginning and at the end of the test overlap with each other. The standard deviation and coefficient of variation (=standard deviation/mean) of the peak wavelength of 2.13 μm are 0.00119 μm and 0.05%, respectively, while the standard deviation and coefficient of variation of the average power of 3.97 mW are 0.085 mW and 2.14%, respectively. These numbers indicate reasonable stability of the system.

VI. Conclusion

In conclusion, the link between chirp prior to amplification and high ECE is established by introducing the concept of soliton order preservation. We demonstrate experimentally how pre-chirping affects the high-order soliton compression in the CF, preserving the soliton order at the input of the NLF within a certain range. The pre-chirp condition is optimized for broad tunability and high ECE by varying the length of the DCF. For a DCF length of 8.0 m, the soliton order at the input of the NLF is preserved within $2.0<N_{NLF}<2.3$, resulting in the preservation of ECE within 80-85% for a tunability as large as 180 nm over the spectral range of 1.96-2.14 μm. Overall, solitons are stable and tunable by up to 320 nm in the wavelength range of 1.96-2.28 μm, and are nearly transform-limited with a minimum TBP of 0.35. A minimum soliton duration of 126 fs is observed. Soliton energy remains above 0.8 nJ for the entire tunable wavelength range, reaching a maximum value of 2.9 nJ. The

intense ultrashort pulses of this wavelength converter could be used in various applications in the 2 μm wavelength band, including but not limited to spectroscopy, sensing, and pump source for mid-infrared supercontinuum generation. The demonstrated soliton order preservation mechanism is of utmost interest for SSFS systems, whether based on active or passive fibers, leading to high ECE while maintaining a broad soliton tunability.

ACKNOWLEDGMENT

The authors are thankful to Coractive for providing the nonlinear and active fibers used in this experiment. M. H. M. Shamim thank Robi Kormokar for his valuable suggestion during the revision of the manuscript.

REFERENCES

[1] R. Kormokar, M. Shamim, and M. Rochette, "High-order analytical formulation of soliton self-frequency shift," *J. Opt. Soc. Am. B*, vol. 38, no. 2, pp. 466–475, 2021.

[2] G. P. Agrawal, *Nonlinear Fiber Optics*, 6th ed. Elsevier, 2019.

[3] A. Al-Kadry and M. Rochette, "Maximized soliton self-frequency shift in non-uniform microwires by the control of third-order dispersion perturbation," *J. Light. Technol.*, vol. 31, no. 9, pp. 1462–1467, 2013.

[4] T. North and M. Rochette, "Broadband self-pulsating fiber laser based on soliton self-frequency shift and regenerative self-phase modulation," *Opt. Lett.*, vol. 37, no. 14, p. 2799, 2012.

[5] O. Szewczyk, P. Pala, K. Tarnowski, J. Olszewski, F. S. Vieira, C. Lu, A. Foltynowicz, P. Mergo, J. Sotor, G. Sobo, and T. Martynkien, "Dual-wavelength pumped highly birefringent microstructured silica fiber for widely tunable soliton self-frequency shift," *J. Light. Technol.*, vol. 39, no. 10, pp. 3260–3268, 2021.

[6] A. M. Al-kadry and M. Rochette, "Mid-infrared sources based on the soliton self-frequency shift," *J. Opt. Soc. Am. B*, vol. 29, no. 6, p. 1347-1355, 2012.

[7] B. Li, M. Wang, K. Charan, M. Li, and C. Xu, "Investigation of the long wavelength limit of soliton self-frequency shift in a silica fiber," *Opt. Express*, vol. 26, no. 15, p. 19637-19647, 2018.

[8] Y. Matsuo, N. Nishizawa, M. Mori, and T. Goto, "Characteristics of wavelength tunable femtosecond soliton pulse generation using femtosecond pump laser and polarization maintaining fiber," *Opt. Rev.*, vol. 7, no. 4, pp. 309–316, 2000.

[9] Y.-H. Chen, P. Sidorenko, E. Antonio-Lopez, R. Amezcua-Correa, and F. Wise, "Efficient soliton self-frequency shift in hydrogen-filled hollow-core fiber," *Opt. Lett.*, vol. 47, no. 2, p. 285, 2022.

[10] I. Alamgir, M. H. M. Shamim, W. Correr, Y. Messaddeq, and M. Rochette, "Mid-infrared soliton self-frequency shift in chalcogenide glass," *Opt. Lett.*, vol. 46, no. 21, p. 5513-5516, 2021.

[11] X. Fang, Z. Wang, and L. Zhan, "Efficient generation of all-fiber femtosecond pulses at 1.7 μm via soliton self-frequency shift," *Opt. Eng.*, vol. 56, no. 4, p. 046107, 2017.

[12] P.Morin, S. Boivinet, J.-P. Yehouessi, S. Vidal, T. Berberian, F. Druon, G. Machinet, F. Guichard, Y. Zaouter, and J. Boullet, "nJ-class all-PM fiber tunable femtosecond laser from 1800 nm to 2050 nm via a highly efficient SSFS," in *Proc. SPIE 11357, 2020*, p. 1135715.

[13] J. Wang, S. Lin, X. Liang, M. Wang, P. Yan, G. Hu, T. Albrow-Owen, S. Ruan, Z. Sun, and T. Hasan, "High-energy and efficient Raman soliton generation tunable from 1.98 to 2.29 μm in an all-silica-fiber thulium laser system," *Opt. Lett.*, vol. 42, no. 18, p. 3518-3521, 2017.

[14] P. Wang, H. Shi, F. Tan, and P. Wang, "Enhanced tunable Raman soliton source between 1.9 and 2.36 μm in a Tm-doped fiber amplifier," *Opt. Express*, vol. 25, no. 14, p. 16643-16651, 2017.

[15] S. Ge, J. Wang, H. Ren, T. Huang, P. Yang, K. Xia, S. Mo, M. Qiu, P. Xu, S. Bai, S. Dai, and Q. Nie, "High-efficiency tunable femtosecond solitons generation from 1.9 to 2.35 μm in a thulium-doped fiber amplifier via precise seed-pulse management," *Opt. Express*, vol. 30, no. 2, pp. 3089–3100, 2022.

[16] J. Luo, B. Sun, J. Ji, E. L. Tan, Y. Zhang, and X. Yu, "High-efficiency femtosecond Raman soliton generation with a tunable wavelength beyond 2 μm," *Opt. Lett.*, vol. 42, no. 8, p. 1568-1571, 2017.

[17] P. Ciąćka, A. Rampur, A. Heidt, T. Feurer, and M. Klimczak, "Dispersion measurement of ultra-high numerical aperture fibers covering thulium, holmium, and erbium emission wavelengths," *J. Opt. Soc. Am. B*, vol. 35, no. 6, p. 1301-1307, 2018.

[18] John A. Buck, *Fundamentals of Optical Fibers*. Wiley, 2004.

[19] D. Milam, "Review and assessment of measured values of the nonlinear refractive-index coefficient of fused silica," Appl. Opt., vol. 37, no. 3, p. 546, 1998.

[20] G. Patwardhan, J. Ginsberg, C. Chen, M. Jadidi, and A. Gaeta, "Nonlinear refractive index of solids in mid-infrared," *Opt. Lett.*, vol. 46, no. 8, p. 1824, 2021.

[21] J. M. Dudley, G. Genty, and S. Coen, "Supercontinuum generation in photonic crystal fiber," *Rev. Mod. Phys.*, vol. 78, no. 4, pp. 1135–1184, 2006.

[22] Y. Wan, J. Luo, and W. Chang, "Tuning the soliton-effect compression via stretching of the pump," *Laser Phys.*, vol. 30, art. no. 105401, 2020.

[23] P. Colman, C. Husko, S. Combrié, I. Sagnes, C. W. Wong, and A. De Rossi, "Temporal solitons and pulse compression in photonic crystal waveguides," *Nat. Photonics*, vol. 4, no. 12, pp. 862–868, 2010.

[24] I. Sorokina, V. Dvoyrin, N. Tolstik, and E. Sorokin, "Mid-IR Ultrashort Pulsed Fiber-Based Lasers," *IEEE J. Sel. Top. Quantum Electron.*, vol. 20, no. 5, pp. 99–110, Sep. 2014.

[25] D. Klimentov, N. Tolstik, V. Dvoyrin, R. Richter, and I. Sorokina, "Flat-Top Supercontinuum and Tunable Femtosecond Fiber Laser Sources at 1.9-2.5 μm," *J. Light. Technol.*, vol. 34, no. 21, pp. 4847–4855, 2016.